PLOS ONE

RESEARCH ARTICLE

End-member modeling of the grain-size record of Sikouzi fine sediments in Ningxia (China) and implications for temperature control of Neogene evolution of East Asian winter monsoon

Hanchao Jiang[1]*, Shiming Wan[2], Xiaolin Ma[3], Ning Zhong[1], Debo Zhao[2]

1 State Key Laboratory of Earthquake Dynamics, Institute of Geology, China Earthquake Administration, Beijing, China, **2** Key Laboratory of Marine Geology and Environment, Institute of Oceanology, Chinese Academy of Sciences, Qingdao, China, **3** State Key Laboratory of Loess and Quaternary Geology, Institute of Earth Environment, Chinese Academy of Sciences, Xi'an, China

* hcjiang@ies.ac.cn

Citation: Jiang H, Wan S, Ma X, Zhong N, Zhao D (2017) End-member modeling of the grain-size record of Sikouzi fine sediments in Ningxia (China) and implications for temperature control of Neogene evolution of East Asian winter monsoon. PLoS ONE 12(10): e0186153. https://doi.org/10.1371/journal.pone.0186153

Editor: Xiaoyan Yang, Chinese Academy of Sciences, CHINA

Received: June 23, 2017

Accepted: September 26, 2017

Published: October 12, 2017

Data Availability Statement: In this study, all data are available as an uploaded file of supplementary data.

Funding: This work was supported by the National Natural Science Foundation of China (grants 41602358, 41572346) and the special project of the fundamental scientific research of the Institute of Geology, China Earthquake Administration (IGCEA1713, IGCEA1508). The funders had no role in study design, data collection and analysis,

Abstract

The Late Cenozoic East Asian winter monsoon (EAWM) enhancement has been attributed to several factors, such as uplift of the Tibetan Plateau, retreat of the Paratethys Sea, and global cooling related to polar ice volume increment. However, the fundamental forcing factors remain enigmatic due to the absence of long and continuous climate records and sensitive indicators. Here we reanalyzed the published grain-size record of Sikouzi fine sediments in the western Chinese Loess Plateau through end-member (EM) modeling. The results indicate that EM 2 with grain-size peaks between 10–100 μm decreased in content from 20.1 to 17 Ma and stepwise increased from 17 to 0.07 Ma during the following six stages (17–15 Ma, 15–12 Ma, 12–8 Ma, 8–6 Ma, 6–4 Ma and 4–0 Ma). Such varying trends can be successively correlated in seven stages with the integrated benthic $\delta^{18}O$ record, implying that global warming weakened the EAWM from 20.1 to 17 Ma and global cooling has stepwise strengthened the EAWM since 17 Ma. Therefore, we conclude that global temperature change played a major role on the evolution of EAWM during the Neogene period. By contrast, Late Cenozoic palaeogeographic reorganization caused by uplift of the Tibetan Plateau and retreat of the Paratethys Sea contributed less to the evolutionary evolution of EAWM. Spectral analysis of the EM 2 data first provided direct evidence of orbitally influenced deposition in the study area and thus the EAWM variations during the Neogene period. The 100-kyr period became weak since ~10 Ma, possibly due to the decrease in sensitivity of a more stable, continental-scale ice sheet in Antarctica to local insolation forcing, deserving further investigation.

decision to publish, or preparation of the manuscript.

Competing interests: The authors have declared that no competing interests exist.

1. Introduction

Dust has extensively deposited in the Chinese Loess Plateau (CLP) at least since the Late Oligocene [1–4]. Most loess deposits are generally underlain by Miocene to Pliocene red clay [4–10]. Both loess and red clay are dominated by silt particles. It is a common sense that the Quaternary loess was generally transported by the East Asian winter monsoon (EAWM) though dry riverbeds have recently been recognized as important dust sources for the CLP and, by inference, for the downwind North Pacific Ocean [11–13]. But the pre-Quaternary dust in the CLP has different interpretations. For example, grain-size records of bulk samples from four sections (Lingtai, Xifeng, Zhaojiachuan and Luochuan) in the central CLP are used to reveal variations in the EAWM and westerly circulation [9] while quartz grain size is selected as a winter monsoon index [10]. Accordingly, a new continuous sensitive record is needed to explore long-term evolution of the EAWM so that its controlling factors can be addressed.

In semi-arid to arid regions, dust particles can be easily trapped by moist surfaces including water bodies and vegetated surfaces like in a basin. A well-exposed, 2880-m-thick fluviolacustrine sequence at Sikouzi, Guyuan, Ningxia, China (Fig 1), suggested that a grand basin long-term developed in the eastern Liupan Mountains in the western CLP during the Neogene period, which was demonstrated generally continuous by magnetostratigraphic investigation, spanning from 20.1 to 0.07 Ma [14]. Rare earth element patterns and sedimentary features of representative samples from the Sikouzi sequence pointed to the windblown origin of Sikouzi fine sediments [15]. This is well consistent with recent provenance recognition of Late Cenozoic lacustrine sediments in North China [16–17]. Although our previous study presented a rough three-stage evolution of the Sikouzi grain-size record [15], detailed numerical analysis was not conducted and more information on climate change remains to be detected.

2. End-member modeling of the grain-size record

Numerical unmixing of grain size distribution data into constituent components, known as end-member analysis (EMA), can yield valuable information on geological processes and palaeo-environmental changes [18–20]. In this study, we reanalyzed the Sikouzi grain-size data composed of 3398 samples [15] using a new developed GUI software of AnalySize for processing and unmixing grain size data [19]. In the correlation map between multiple correlation coefficient (R^2) and end-member number (Fig 2A), end-member modeling improved greatly from 2 to 3 end members, but improved fairly less from 3 to 4 end members. Given that explaining the observed compositional variation requires a minimum number of end members in EMA [18], three end members were modeled in this study and their peak values concentrated at 1–10 μm (EM 1), 10–100 μm (EM 2), and more than 100 μm (EM 3), respectively (Fig 2B). Noticeably, the study area lies in the western CLP and remained arid to semi-arid during the Neogene period [21–22], which is supported by the spatial and temporal variations in *Fupingopollenites* percentages across Inner and East Asia [23]. Previous studies suggest that the clay mineral composition in loess and soil was of clastic origin [24] and that some clay-size material is formed in low energy aeolian environments [25] or mountain processes such as glacial grinding, frost weathering, salt weathering and even earthquakes [26–30], and thus variation in EM 1 reflected a background deposition of dust. By contrast, abundance fluctuation in EM 2 probably indicated variations in the East Asian winter monsoon (EAWM) and the EM 3 fraction probably came from nearby the study area [15]. Correspondingly, 44 representative samples of Sikouzi fine sediments were selected and divided into three groups, and their relative and accumulative frequency curves were presented in Fig 3. They seemingly reflect different dynamics of transportation.

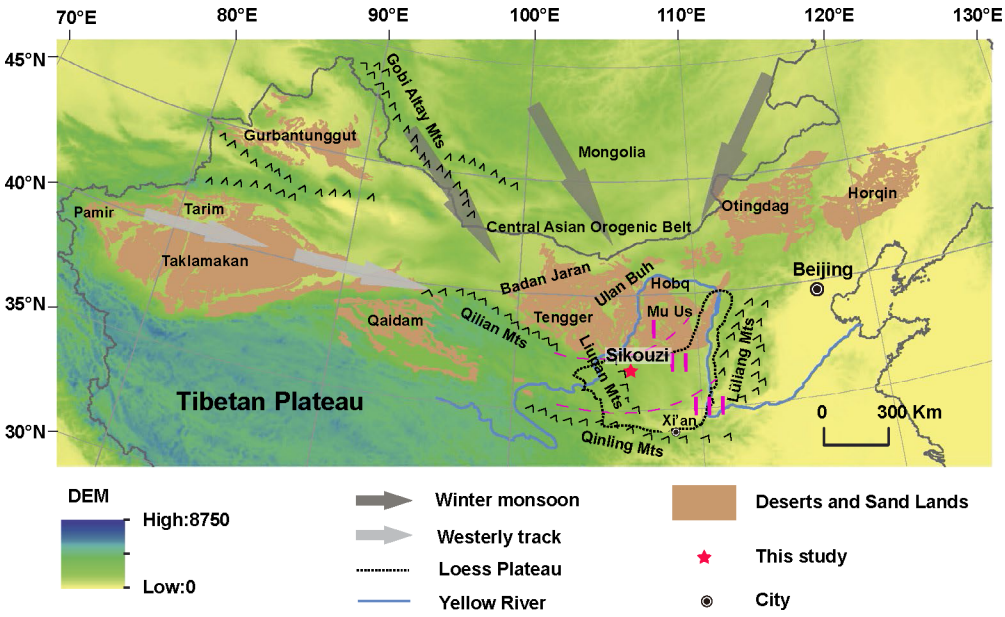

Fig 1. Digital elevation model (DEM) map of northern China. Zone I-sandy loess; zone II-loess; zone III-clayey loess. The decrease in loess grains from northwest to southeast is consistent with the northwesterly winter monsoon winds over East Asia. The desert and mountains are indicated (adapted from [55]).

https://doi.org/10.1371/journal.pone.0186153.g001

3. Provenance analysis of C-M pattern

C-M patterns comprised by the one percentile (C) and the median diameter (M) are characteristic of the depositional agent [31], and different parts of a C-M pattern reflect different processes of transportation and deposition [32]. We compared our 44 representative samples with the Mississippi river ones [31] in Fig 3. Distribution of the Mississippi river samples showed an L shape with knee point closest to the C = M line, indicating that only a few of river samples had a relatively good sorting. In contrast, 44 Sikouzi fine samples (Fig 3), and even almost all of the Sikouzi samples, whether the fine (C < 135 μm) or the relatively coarse (C > 135 μm) ones (Fig 4), are parallel to sub-parallel with the C = M line, implying that they had much better sorting than the Mississippi river samples [31–32]. This further supports the windblown origin of Sikouzi fine sediments [15], and is also consistent with our recent major and minor

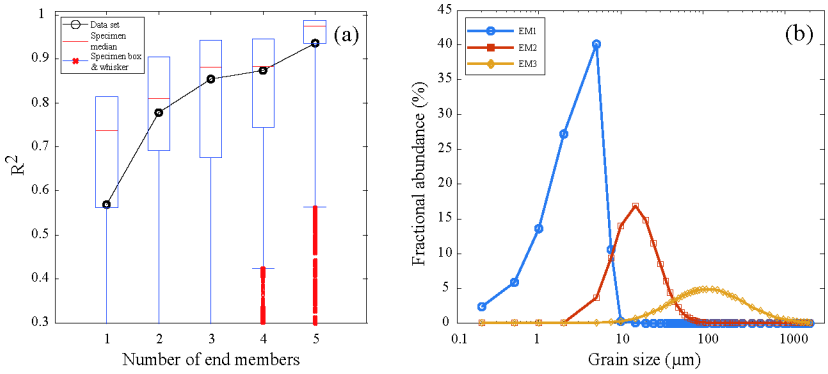

Fig 2. Correlation map between multiple correlation coefficient (R^2) and number of end-member (a), and three selected end members (b).

https://doi.org/10.1371/journal.pone.0186153.g002

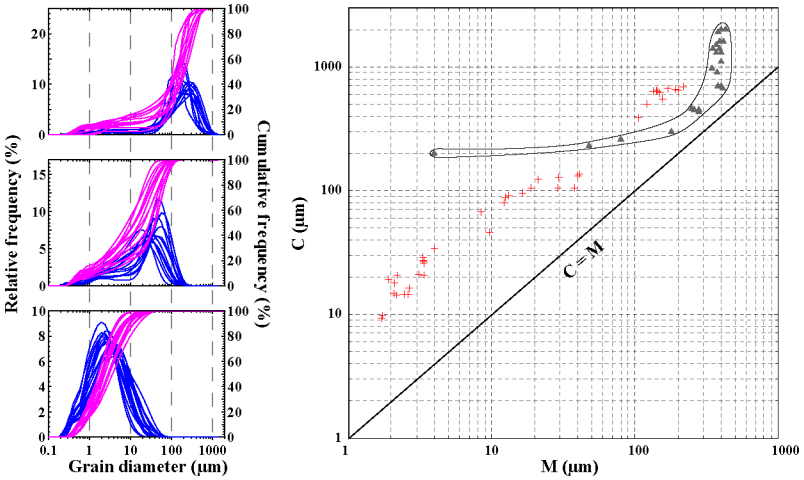

Fig 3. Relative and accumulative frequency of 44 representative samples selected from the Sikouzi grain-size sequence are correlative to 3 end members in Fig 2, and their distribution in a C-M plot (red cross) is in contrast with that of the Mississippi river samples (gray triangles, [31]). The former is parallel to line C = M while the latter shows an L shape.

https://doi.org/10.1371/journal.pone.0186153.g003

element analysis (under submission). Furthermore, C values are usually more than 200 μm for river samples and M values are often less than 10 μm for deep sea or deep lake samples [32]. These samples distribute in different areas from our samples. Thus these distribution features can readily differ the Sikouzi windblown sediments from river or deep lake ones.

Therefore, the relatively coarse ones with C values > 135 μm (only 290 in all, ~8.5% of the total 3398 samples), like the relatively fine ones with C values < 135 μm, are possibly wind-blown in origin as well, because they are concentrated in the CM plot and are parallel to the C = M line (Fig 4), showing a feature of good sorting for aeolian deposit. These relatively coarse particles were probably transported by ambient wind [33–35] or gust [36] from nearby sources.

4. Discussion

In this study, each of three end-members varied from zero to 100% but had different averages (Fig 5). EM 1 had a mean value of 47.4% while EM 2 had an average of 38.4%. By contrast, EM

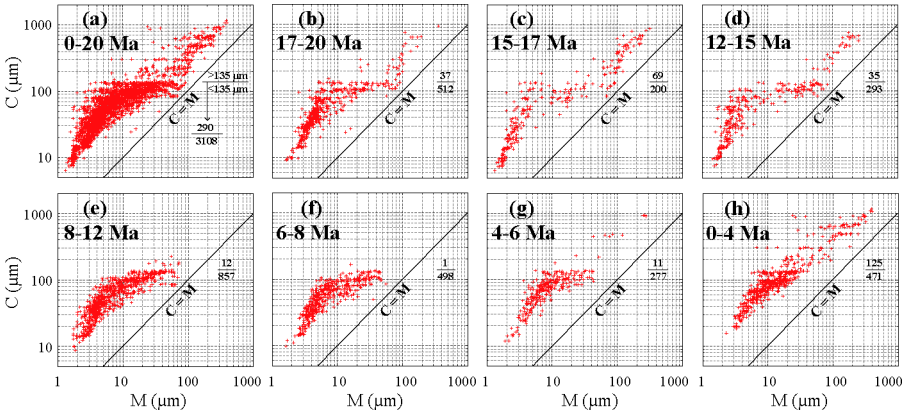

Fig 4. Grain size distribution of the Sikouzi fine samples in a C-M plot during past 20 Ma and during different time intervals.

https://doi.org/10.1371/journal.pone.0186153.g004

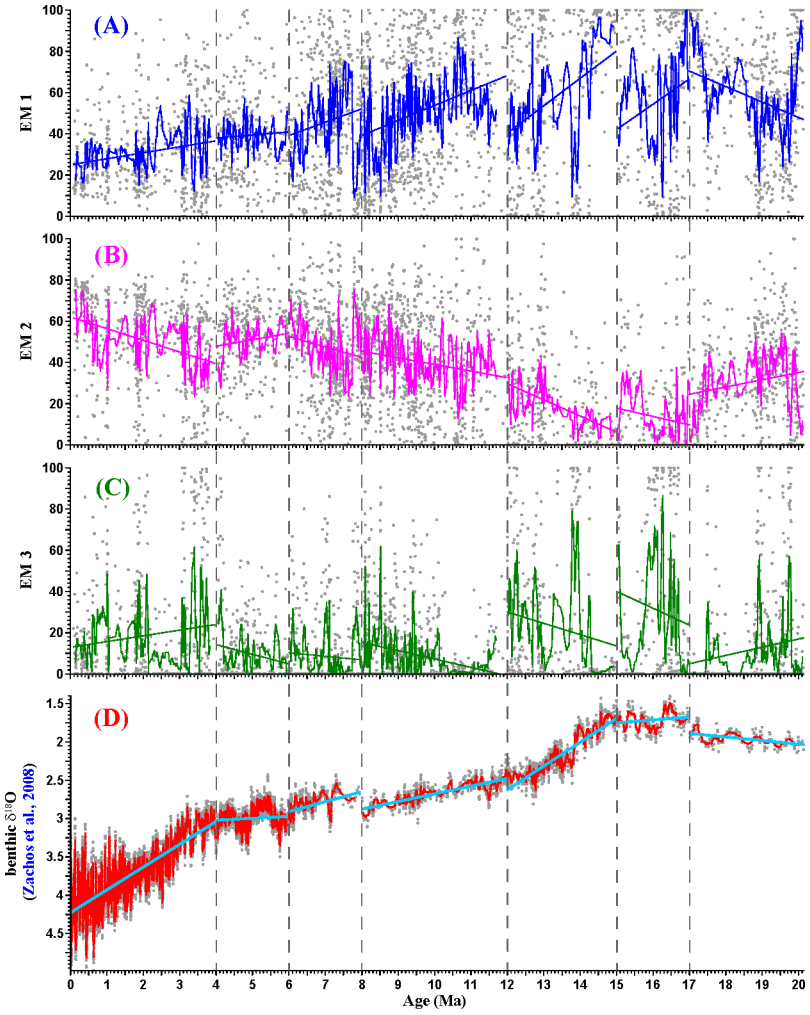

Fig 5. Variations of three end members of the Sikouzi grain-size sequence spanning the past 20 Ma plotted against paleomagnetic ages and its correlation with the integrated $\delta^{18}O$ curve [37]. For each time interval, the solid line is linear fitting and the solid curve is averaging with a window width of 11 data points.

https://doi.org/10.1371/journal.pone.0186153.g005

3 had a low mean value of 14.2%. In order to present a clear varying trend for each end-member, we run a linear fitting and averaging with a window width of 11 data points for each time interval. EM 1 generally increased in abundance from 20.1 to 17 Ma and stepwise decreased from 17 to 0.07 Ma (Fig 5A). On the contrary, percentage of EM 2 decreased from 20.1 to 17 Ma and stepwise increased from 17 to 0.07 Ma (Fig 5B). Intriguingly, EM 3 also showed a similar varying trend to EM 2 except the last time interval since 4 Ma (Fig 5C).

Such clear varying trends for three end-members of the Sikouzi grain-size record in Ningxia can be well correlated with the benthic foraminiferal composite $\delta^{18}O$ record [37] (Fig 5D). Given that shifts in $\delta^{18}O$ are believed to reflect changes in global ice volume and thus variations in global temperature [37–39], we believe that shifts in $\delta^{18}O$ were tightly associated with changes in global temperature during the late Cenozoic period. From 20.1 to 17 Ma, both EM 2 and the $\delta^{18}O$ curve showed a decreasing trend, implying that global warming during this period weakened the EAWM. From 17 to 0.07 Ma, the $\delta^{18}O$ curve, EM 2, and EM 3 showed a stepwise increasing trend (Fig 5), implying that global cooling stepwise strengthened the EAWM since 17 Ma. The middle-late Miocene transition and the significant development of

East Antarctic Ice Sheet probably not only strengthened the meridional temperature gradients and global aridity in the middle-high latitudes, but also intensified the oceanic and atmospheric circulation and the major falling of global sea level [21–22]. Several positive feedback mechanisms possibly modulated and magnified the mid-Miocene global cooling, including vegetation changes, greenhouse gas (atmospheric CO_2 and water vapor) fluctuations as Jiang et al. [39] proposed.

Noticeably, from 6 to 4 Ma, whether the $\delta^{18}O$ curve, EM 2 or EM 1, showed a slow variation or maintained relatively stable, probably because the climate in Asia corresponded to global warming during the Early Pliocene [40–41]. Supporting this viewpoint, sea surface temperature had almost no cooling from 6 to 4 Ma in the northwestern Pacific [42].

From 4 to 0.07 Ma, both the $\delta^{18}O$ curve and EM 2 showed a rapid increase to the highest values while EM 1 declined to the lowest for the whole sequence (Fig 5), indicating prominent increase in polar ice volume was responsible for significant strengthening of the EAWM over the past 4 Ma [15, 37].

Under the age control of biostratigraphy and magnetostratigraphy [14], the EM 2 data of the Sikouzi grain-size record were detrended with a first difference filter to remove low-frequency variance. We used the REDFIT38 program [43] to analyze the EM 2 data deducted by LOESS (locally weighted scatterplot smoothing). Spectral analysis shows a clear forcing at eccentricity (405 kyr and 100 kyr) and obliquity (41 kyr) (Fig 6A), for the first time providing direct evidence of orbitally influenced fluctuating cycles of dust deposition in the study area and thus the EAWM variations during the Neogene period. Furthermore, we used the wtc-r16 Matlab package to conduct continuous wavelet analysis [44] on the detrended EM 2 data. The results show that the 405-kyr period was generally strong over the past 20 Ma and got obviously stronger during the Middle Miocene Climate Optimum (MMCO). Interestingly, during the same period, both the benthic and planktonic $\delta^{13}C$ records at Site U1337 in the east equatorial Pacific reveal marked 405-kyr carbon isotope cycles [45] as in ocean carbon reservoir [46], probably indicating that the long eccentricity (405-kyr) paced carbon inputs from terrestrial weathering to ocean [45] and possibly drove the East Asian summer monsoon [47]. The 100-kyr period became weak after ~10 Ma (Fig 6B), possibly due to the decrease in sensitivity of a more stable, continental-scale ice sheet in Antarctica to local insolation forcing [48]. Noticeably, the 100-kyr period became strong at ~8.5–7 Ma, which is well correlated with the analyzed results of Late Miocene lacustrine record from the eastern Qaidam Basin in Northwest China [49], possibly due to Southern Hemisphere insolation-driven Antarctic ice sheet forcing or ephemeral variations of the Northern Hemispherie ice sheets before 7 Ma [50–51]. This inference is well consistent with the enhanced amplitude variation of the 100-kyr period during the Mi events [52], implying that the 100-kyr cycle was strengthened at times of glacial maxima as they were during the Late Pleistocene. Since ~5 Ma, the 100-kyr period showed a higher variability than before, which is probably associated with the development and fluctuation of bipolar ice volume [47, 53–54]. These deserve further investigation in the future.

5. Conclusion

EMA of the grain-size record of Sikouzi lacustrine sediments in Ningxia indicates that the varying trend of three end members can be successively correlated in seven stages with the integrated benthic $\delta^{18}O$ record, implying that global warming weakened the EAWM from 20.1 to 17 Ma and global cooling stepwise strengthened the EAWM since 17 Ma. Hence, we conclude that global temperature related to polar ice volume played a major role on the long-term evolution of EAWM during the Neogene period. By comparison, Late Cenozoic palaeogeographic reorganization caused by uplift of the Tibetan Plateau and retreat of the

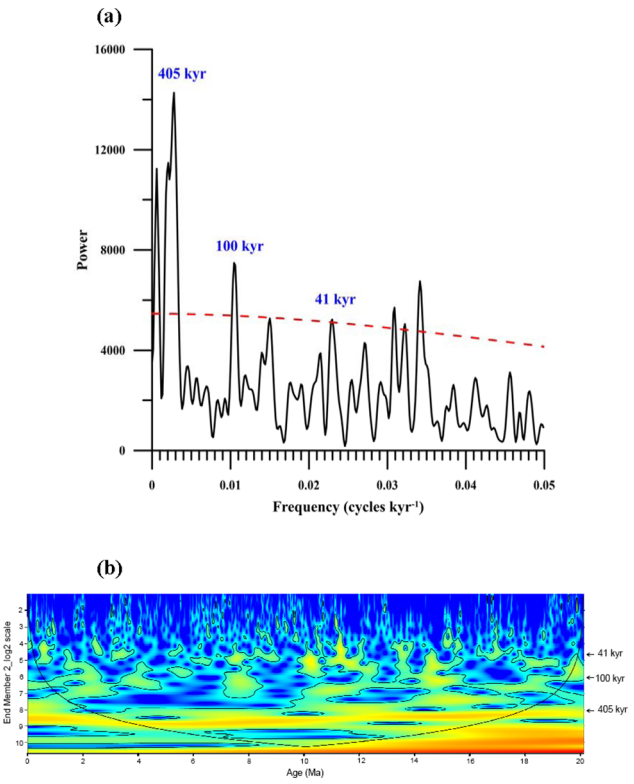

Fig 6. Power (a) and evolutive (b) spectrums over the past 20 Ma on the detrended EM 2 data of Sikouzi grain-size record. Note that the 405-kyr period kept strong over the past 20 Ma and the 100-kyr period weakened since ~10 Ma.

https://doi.org/10.1371/journal.pone.0186153.g006

Paratethys Sea contributed less to the long-term evolution of EAWM. Spectral analysis of the EM 2 data first provided direct evidence of orbitally influenced deposition of dust particles in the study area and thus the EAWM variations during the Neogene period. The 100-kyr period weakened since ~10 Ma, possibly due to the decrease in sensitivity of a more stable, continental-scale ice sheet in Antarctica to local insolation forcing, deserving further investigation.

Funding

This work was supported by the National Natural Science Foundation of China (grants 41602358, 41572346) and the special project of the fundamental scientific research of the Institute of Geology, China Earthquake Administration (IGCEA1713, IGCEA1508). The funders had no role in study design, data collection and analysis, decision to publish, or preparation of the manuscript.

Supporting information

S1 Data. End-member abundances and densities of the Sikouzi grain-size sequence.
(XLS)

Acknowledgments

We feel grateful to Prof. Xiaoyan Yang (editor) and two anonymous reviewers for valuable comments. Data supporting the paper are available in supporting information.

Author Contributions

Conceptualization: Hanchao Jiang.

Data curation: Xiaolin Ma, Debo Zhao.

Formal analysis: Ning Zhong, Debo Zhao.

Investigation: Xiaolin Ma.

Methodology: Shiming Wan, Ning Zhong.

Software: Shiming Wan, Debo Zhao.

Writing – review & editing: Hanchao Jiang.

References

1. Guo ZT, Ruddiman WF, Hao QZ, Wu HB, Qiao YS, Zhu RX, et al. (2002) Onset of Asian desertification by 22 Myr ago inferred from loess deposits in China. Nature 416: 159–163. https://doi.org/10.1038/416159a PMID: 11894089
2. Qiang XK, An ZS, Song YG, Chang H, Sun YB, Liu WG, et al. (2011) New eolian red clay sequence on the western Chinese Loess Plateau linked to onset of Asian desertification about 25 Ma ago. Sci. China Earth Sci. 54: 136–144.
3. Zhang YB, Sun DH, Li ZJ, Wang F, Wang X, Li BF, et al. (2014) Cenozoic record of aeolian sediment accumulation and aridification from Lanzhou, China, driven by Tibetan Plateau uplift and global climate. Global and Planetary Change 120: 1–15.
4. Sun YB, Ma L, Bloemendal J, Clemens S, Qiang XK, and An ZS (2015) Miocene climate change on the Chinese Loess Plateau: Possible links to the growth of the northern Tibetan Plateau and global cooling. Geochem. Geophys. Geosyst. 16: 2097–2108.
5. Ding ZL, Rutter N, Liu TS (1993) Pedostratigraphy of Chinese loess deposits and climatic cycles in the last 2.5 Myr. CATENA 20: 73–91.
6. Ding ZL, Sun JM, Yang SL and Liu TS (1998) Preliminary magnetostratigraphy of a thick eolian red clay-loess sequence at Lingtai, the Chinese Loess Plateau. Geophys. Res. Lett. 25: 1225–1228.
7. Ding ZL, Xiong SF, Sun JM, Yang SL, Gu ZY, Liu TS (1999) Pedostratigraphy and paleomagnetism of a ~7.0 Ma eolian loess-red clay sequence at Lingtai, Loess Plateau, north-central China and the implications for paleomonsoon evolution. Palaeogeogr. Palaeoclimatol. Palaeoecol. 152: 49–66.
8. Ding ZL, Rutter NW, Sun JM, Yang SL, Liu TS (2000) Re-arrangement of atmospheric circulation at about 2.6 Ma over northern China: evidence from grain size records of loess-palaeosol and red clay sequences. Quat. Sci. Rev. 19: 547–558.
9. Sun DH, Su RX, Bloemendal J, Lu HY (2008) Grain-size and accumulation rate records from Late Cenozoic aeolian sequences in northern China: Implications for variations in the East Asian winter monsoon and westerly atmospheric circulation. Palaeogeogr. Palaeoclimatol. Palaeoecol. 264: 39–53.
10. Sun YB, An ZS, Clemens SC, Bloemendal J, Vandenberghe J (2010) Seven million years of wind and precipitation variability on the Chinese Loess Plateau. Earth Planet. Sci. Lett. 297: 525–535.
11. Stevens T, Carter A, Watson TP, Vermeesch P, Ando S, Bird AF, et al. (2013) Genetic linkage between the Yellow River, the Mu Us desert and the Chinese Loess Plateau. Quat. Sci. Rev. 78: 355–368.
12. Nie JS, Stevens T, Rittner M, Stockli D, Garzanti E, Limonta M, et al. (2015) Loess Plateau storage of northeastern Tibetan Plateau-derived Yellow River sediment. Nature Communications 6:8511, https://doi.org/10.1038/ncomms9511 PMID: 26449321
13. Licht A, Pullen A, Kapp P, Abell J, and Giesler N (2016) Eolian cannibalism: Reworked loess and fluvial sediment as the main sources of the Chinese Loess Plateau. Geol. Soc. Am. Bull. 128: 944–956.
14. Jiang HC, Ding ZL, Xiong SF (2007) Magnetostratigraphy of the Neogene Sikouzi section at Guyuan, Ningxia, China. Palaeogeogr. Palaeoclimatol. Palaeoecol. 243: 223–234.
15. Jiang HC, Ding ZL (2010) Eolian grain-size signature of the Sikouzi lacustrine sediments (Chinese Loess Plateau): Implications for Neogene evolution of the East Asian winter monsoon. Geol. Soc. Am. Bull. 122: 843–854.
16. Zhai QM, Guo ZY, Li YL, Li RQ (2006) Annually laminated lake sediments and environmental changes in Bashang Plateau, North China. Palaeogeogr. Palaeoclimatol. Palaeoecol. 241: 95–102.

17. Jiang HC, Guo GX, Cai XM, Thompson JA, Xu HY, Zhong N (2016) Geochemical evidence of wind-blown origin of the LateCenozoic lacustrine sediments in Beijing and implications for weathering and climate change. Palaeogeogr. Palaeoclimatol. Palaeoecol. 446: 32–43.
18. Weltje GJ (1997) End-member modeling of compositional data: Numerical-statistical algorithms for solving the explicit mixing problem. Math. Geol. 29: 503–549.
19. Paterson GA and Heslop D (2015) New methods for unmixing sediment grain size data. Geochem. Geophys. Geosys. 16: 4494–4506.
20. Yu SY, Colman SM, Li LX (2016) BEMMA: A Hierarchical Bayesian end-member modeling analysis of sediment grain-size distributions. Mathematical Geosci. 48: 723–741.
21. Jiang HC, Ding ZL (2008) A 20 Ma pollen record of East-Asian summer monsoon evolution from Guyuan, Ningxia, China. Paleogeogr. Paleoclimatol. Paleoecol. 265: 30–38.
22. Jiang H, Ding Z (2009) Spatial and temporal characteristics of Neogene palynoflora in China and its implication for the spread of steppe vegetation. J. Arid Environ. 73: 765–772.
23. Miao YF, Song CH, Fang XM, Meng QQ, Zhang P, Wu FL, et al. (2016) Late Cenozoic genus *Fupingopollenites* development and its implications for the Asian summer monsoon evolution. Gondwana Res. 29: 320–333.
24. Ji JF, Chen J, and Lu HY (1999) Origin of illite in the loess from the Luochuan area, Loess Plateau, Central China. Clay Minerals 34: 525–532.
25. Whalley WB, Marshall JR & Smith BJ (1982) Origin of desert loess from some experimental observations. Nature 300: 433–435.
26. Derbyshire E, Meng XM, and Kemp RA (1998) Provenance, transport and characteristics of modern eolian dust in western Gansu Province, China, and interpretation of the Quaternary loess record. J. Arid Environ. 39: 497–516.
27. Sun JM (2002) Provenance of loess material and formation of loess deposits on the Chinese Loess Plateau. Earth Planet. Sci. Lett. 203: 845–859.
28. Sun JM (2002) Source regions and formation of the loess sediments on the high mountain regions of northwestern China. Quat. Res. 58: 341–351.
29. Jiang HC, Mao X, Xu HY, Yang HL, Ma XL, Zhong N, et al. (2014) Provenance and earthquake signature of the last deglacial Xinmocun lacustrine sediments at Diexi, East Tibet. Geomorphology 204: 518–531.
30. Liang LJ and Jiang HC (2017) Geochemical composition of the last deglacial lacustrine sediments in East Tibet and implications for provenance, weathering and earthquake events. Quat. Int. 430: 41–51.
31. Passega R (1957) Texture as characteristic of clastic deposition. Amer. Assoc. Petroleum Geologists Bull. 41: 1952–1984.
32. Passega R (1964) Grain size representation by CM patterns as a geological tool. J. Sediment. Petrol. 34: 830–847.
33. Chen FH, Qiang MR, Zhou AF, Xiao S, Chen JH, Sun DH (2013) A 2000-year dust storm record from Lake Sugan in the dust source area of arid China. J. Geophys. Res. 118: 1–12.
34. Li Y, Song YG, Nie JS, Sun BY (2014) Tracing the provenance of loess and red clay on the Chinese Loess Plateau using the U-Pb dating and single-size zircon size. Geol. Rev. 60: 380–388 (in Chinese with English abstract).
35. Zhong N, Song XS, Xu HY, Jiang HC (2017) Influence of a tectonically active mountain belt on its foreland basin: Evidence from detrital zircon dating of bedrocks and sediments from the eastern Tibetan Plateau and Sichuan Basin, SW China. J. Asian Earth Sci. 146: 251–264.
36. Muhs DR, Arthur Bettis E III, Roberts HM, Harlan SS, Paces JB, Reynolds RL (2013) Chronology and provenance of last-glacial (Peoria) loess in western Iowa and paleoclimatic implications. Quat. Res. 80: 468–481.
37. Zachos JC, Dickens GR, and Zeebe RE (2008) An early Cenozoic perspective on greenhouse warming and carbon-cycle dynamics. Nature 451: 279–283. https://doi.org/10.1038/nature06588 PMID: 18202643
38. Zachos J, Pagani M, Sloan L, Thomas E, Billups K (2001) Trends, rhythms, and aberrations in global climate 65 Ma to present. Science 292: 686–693. https://doi.org/10.1126/science.1059412 PMID: 11326091
39. Jiang HC, Ji JL, Gao L, Tang ZH, Ding ZL (2008) Cooling-driven climate change at 12–11 Ma: Multiproxy records from a long fluviolacustrine sequence at Guyuan, Ningxia, China. Paleogeogr. Paleoclimatol. Paleoecol. 265: 148–158.

40. Dowsett HJ, Cronin TM, Poore RZ, Thompson RS, Whatley RC, Wood AM (1992) Micropaleontological evidence for increased meridional heat transport in the North Atlantic Ocean during the Pliocene. Science 258: 1133–1135. https://doi.org/10.1126/science.258.5085.1133 PMID: 17789085

41. Hermoyian CS and Owen RM (2001) Late Miocene-early Pliocene biogenic bloom: Evidence from low-productivity regions of the Indian and Atlantic Oceans. Paleoceanography 16: 95–100.

42. LaRiviere JP, Christina Ravelo A, Crimmins A, Dekens PS, Ford HL, Lyle M, et al. (2012) Late Miocene decoupling of oceanic warmth and atmospheric carbon dioxide forcing. Nature 486: 97–100. https://doi.org/10.1038/nature11200 PMID: 22678287

43. Schulz M and Mudelsee M (2002) REDFIT: Estimating red-noise spectra directly from unevenly spaced paleoclimatic time series. Comput. Geosci. 28: 421–426.

44. Grinsted A, Moore JC and Jevrejeva S (2004) Application of the cross wavelet transform and wavelet coherence to geophysical time series. Nonlinear Processes in Geophysics 11: 561–566.

45. Tian J, Ma WT, Lyle MW, Shackford JK (2014) Synchronous mid-Miocene upper and deep oceanic δ13C changes in the east equatorial Pacific linked to ocean cooling and ice sheet expansion. Earth Planet. Sci. Lett. 406: 72–80.

46. Ma WT, Tian J, Li QY and Wang PX (2011) Simulation of long eccentricity (400-kyr) cycle in ocean carbon reservoir during Miocene Climate Optimum: Weathering and nutrient response to orbital change. Geophys. Res. Lett. 38: L10701, https://doi.org/10.1029/2011GL047680

47. Tian J, Xie X, Ma WT, Jin HY, and Wang PX (2011) X-ray fluorescence core scanning records of chemical weathering and monsoon evolution over the past 5 Myr in the southern South China Sea. Paleoceanography 26: PA4202, https://doi.org/10.1029/2010PA002045

48. Galeotti S, DeConto R, Naish T, Stocchi P, Florindo F, Pagani M, et al. (2016) Antarctic Ice Sheet variability across the Eocene-Oligocene boundary climate transition. Science 352: 76–80. https://doi.org/10.1126/science.aab0669 PMID: 27034370

49. Nie JS, Garzione C, Su QD, Liu QS, Zhang R, Heslop D, et al. (2017) Dominant 100,000-year precipitation cyclicity in a late Miocene lake from northeast Tibet. Science Advances 3:e1600762. https://doi.org/10.1126/sciadv.1600762 PMID: 28435857

50. Eldrett JS, Harding IC, Wilson PA, Butler E, Roberts AP (2007) Continental ice in Greenland during the Eocene and Oligocene. Nature 446: 176–179. https://doi.org/10.1038/nature05591 PMID: 17287724

51. John KSt (2008) Cenozoic ice-rafting history of the central Arctic Ocean: Terrigenous sands on the Lomonosov Ridge. Paleoceanogrpahy 23: PA1S05.

52. Beaufort L (1994) Climate importance of the modulation of the 100 kyr cycle inferred from 16 m.y. long Miocene records. Paleoceanography 9: 821–834.

53. Thiede J, Winkler A, Wolf-Welling T, Eldholm O, Myhre AM, Baumann K-H, et al. (1998) Late Cenozoic history of the polar North Atlantic: Results from ocean drilling. Quat. Sci. Rev. 17: 185–208.

54. Jiang HC, Mao X, Xu HY, Thompson J, Ma XL (2010) ~4 Ma coarsening of sediments from Baikal, Chinese Loess Plateau and South China Sea and implications for the onset of NH glaciation. Palaeogeogr. Palaeoclimatol. Palaeoecol. 298: 201–209.

55. Shang Y, Beets CJ, Tang H, Prins MA, Lahaye Y, Elsas R, et al. (2016) Variations in the provenance of the late Neogene Red Clay deposits in northern China. Earth Planet. Sci. Lett. 439: 88–100.